assumed that the effect of uncoupling on the load dominates over the effect of uncoupling on the source. This nonsymmetrical effect can be explained by local differences in the characteristics of depolarizing current flow in the strand versus the expansion: current flow in the strand is highly parallel, resulting in a planar activation wavefront, but it fans out into the expansion, giving rise to a curved activation wavefront. As suggested by recent computer simulations (*14, 15*), this difference in dimensionality of depolarizing current flow has the consequence that uncoupling has a smaller effect on the current source (reduction in one dimension) than on the current load (reduction in two dimensions), thus favoring the establishment of successful conduction. Even though the findings of this study are based on two-dimensional preparations, they are valid for three-dimensional tissue as well (*15*).

The results presented show that if a cellular network contains structural discontinuities, the modification of intercellular electrical coupling can have effects on impulse propagation that are largely different from those encountered in linear or continuous excitable structures. In general, the results show that a decrease of diffusion can support propagation of activation in discontinuous excitable media. For cardiac tissue, this might have the consequence that uncoupling, which is known to be involved in the generation of clinically relevant cardiac arrhythmias (*6*), might also exert anti-arrhythmic effects; even though cellular uncoupling induces an arrhythmogenic slowing of conduction, the possibility of a concurrent suppression of unidirectional conduction blocks in tissue regions with discontinuous structures would, contrary to present expectations, decrease the probability of occurrence of reentrant excitation.

REFERENCES AND NOTES

1. A. T. Winfree, *When Time Breaks Down* (Princeton Univ. Press, Princeton, NJ, 1987).
2. J. M. Davidenko, A. V. Pertsov, R. Salomonsz, W. Baxter, J. Jalife, *Nature* **355**, 349 (1992).
3. I. J. Le Grice *et al.*, *Am. J. Physiol.* **38**, H571 (1995).
4. R. D. Veenstra, R. W. Joyner, D. A. Rawling, *Circ. Res.* **54**, 500 (1984).
5. P. C. Ursell, P. I. Gardner, A. Albala, J. J. Fenoglio, A. L. Wit, *ibid.* **56**, 436 (1985); J. H. Smith, C. R. Green, N. S. Peters, S. Rothery, N. J. Severs, *Am. J. Pathol.* **139**, 801, (1991).
6. M. J. Janse and A. L. Wit, *Physiol. Rev.* **69**, 1049 (1989).
7. Geometrically defined patterns of cultured neonatal rat ventricular myocytes were obtained by means of a previously described method [S. Rohr, D. M. Schölly, A. G. Kléber, *Circ. Res.* **68**, 114 (1991)]. The patterns used in the experiments consisted of cell strands (25 to 70 μm wide and 1.8 mm long) connected to a large rectangular cell monolayer (2.2 by 2.2 mm). The preparations were mounted on an inverted microscope equipped for epifluorescence and were superfused with Hank's balanced salt solution (pH 7.40 at 36°C).
8. The preparations were stained with the voltage-sensitive dye di-8-ANEPPS (Molecular Probes, Eugene, OR), and propagating action potentials were elicited at a basic cycle length of 500 ms with extracellular stimulation electrodes at a distance of >1 mm from the recording area. Changes in transmembrane voltage were monitored with a system for multiple site optical recording of transmembrane voltage with a total of 80 detectors. Optically recorded signals at a given site were normalized to signal amplitudes measured at the same site during control retrograde propagation. If an average action potential amplitude of 100 mV is assumed, the values of these normalized signals translate directly into millivolts. Activation times were determined from the time when the signal at a given site reached 50% of the full amplitude [S. Rohr, *J. Cardiovasc. Electrophysiol.* **6**, 551 (1995)].
9. S. Rohr and B. M. Salzberg, *J. Gen. Physiol.* **104**, 287 (1994); V. G. Fast and A. G. Kléber, *Cardiovasc. Res.* **29**, 697 (1995).
10. The superfusion of defined regions of the preparation was performed with a system described elsewhere [J. Streit and H. D. Lux, *J. Neurosci.* **9**, 4190 (1989)]. The superfusion solution consisted of normal bath medium containing 10 μM palmitoleic acid (dispersed by ultrasonication) and 20 mM sucrose, which rendered the superfusion visible through birefringence.
11. I. Miura, Y. Nasa, K. Ichihara, Y. Abiko, *Clin. Exp. Pharmacol. Physiol.* **18**, 259 (1991).
12. J. M. Burt, K. D. Massey, B. N. Minnich, *Am. J. Physiol.* **260**, C439 (1991).
13. S. Rohr, J. P. Kucera, V. G. Fast, A. G. Kléber, data not shown.
14. C. Cabo *et al.*, *Circ. Res.* **75**, 1014 (1994).
15. V. G. Fast and A. G. Kléber, *Cardiovasc. Res.* **30**, 449 (1995).
16. H. Akima, *Assoc. Comput. Mach. Trans. Math. Software* **4**, 148 (1978).

17. We thank R. Flückiger Labrada for preparing the heart cell cultures and H.-R. Lüscher, J. A. S. McGuigan, E. Niggli, A. L. Obaid, and J. S. Shiner for their helpful comments on the manuscript. Supported by the Swiss National Science Foundation and the Swiss Heart Foundation.

4 November 1996; accepted 3 December 1996

Calcium Waves in Retinal Glial Cells

Eric A. Newman* and Kathleen R. Zahs

Calcium signals were recorded from glial cells in acutely isolated rat retina to determine whether Ca^{2+} waves occur in glial cells of intact central nervous system tissue. Chemical (adenosine triphosphate), electrical, and mechanical stimulation of astrocytes initiated increases in the intracellular concentration of Ca^{2+} that propagated at ~23 micrometers per second through astrocytes and Müller cells as intercellular waves. The Ca^{2+} waves persisted in the absence of extracellular Ca^{2+} but were largely abolished by thapsigargin and intracellular heparin, indicating that Ca^{2+} was released from intracellular stores. The waves did not evoke changes in cell membrane potential but traveled synchronously in astrocytes and Müller cells, suggesting a functional linkage between these two types of glial cells. Such glial Ca^{2+} waves may constitute an extraneuronal signaling pathway in the central nervous system.

Glial cells, long considered to be passive elements in the central nervous system (CNS), are now known to generate active responses (*1*), including intracellular Ca^{2+} signals (*2*). Stimulation of astrocytes triggers increases in the intracellular Ca^{2+} concentration ($[Ca^{2+}]_i$) that can propagate as waves between cells coupled by gap junctions (*3, 4*). These glial Ca^{2+} waves have been observed only in dissociated cell (*3–7*) and organotypic (*8*) culture preparations, which differ from cells in situ in several respects (*9*). Because these waves may represent a form of intercellular signaling in the CNS (*5*) and can potentially modulate neuronal activity (*10, 11*), we tested whether Ca^{2+} waves occur in situ in glial cells of acutely isolated rat retina.

The rat retina contains two types of macroglial cells: astrocytes, which form a two-dimensional syncytium at the vitreal surface of the retina, and Müller cells, which are radial glial cells whose end feet terminate at the vitreal surface and whose trunks project downward into the retina (*12*). We detected $[Ca^{2+}]_i$ in these cells with the fluorescent Ca^{2+} indicator dye Calcium Green-1 (*13*). The vitreal surfaces of flat-mounted retinas were imaged with video-rate confocal microscopy (*14*). Both astrocytes and Müller cells incorporated the dye and were identified by their morphology (Fig. 1A).

Stimulation of a single astrocyte evoked increases in $[Ca^{2+}]_i$ in the simulated cell and in neighboring astrocytes and Müller cells. This Ca^{2+} response propagated outward from the site of stimulation as a wave across the retinal surface (Fig. 1, B to D). Chemical, electrical, and mechanical stimuli were all effective in initiating Ca^{2+} waves. Pressure ejection of adenosine triphosphate (ATP) (200 μM), carbachol (1 mM), or phenylephrine (100 μM) from micropipettes onto astrocyte somata initiated Ca^{2+} waves. In contrast to findings in cultured cells (*2, 5, 15*), local ejection of glutamate (2 mM) or its application in the

Department of Physiology, University of Minnesota, 435 Delaware Street, SE, Minneapolis, MN 55455, USA.

* To whom correspondence should be addressed.

bath (0.3 to 1 mM) was ineffective at evoking $[Ca^{2+}]_i$ increases, but bath application (10 to 100 μM) did potentiate the Ca^{2+} responses initiated by other stimuli. Both electrical stimulation (−2 μA, 40 to 200 ms, delivered through a micropipette) of astrocyte end feet or somata and mechanical stimulation (5- to 10-μm movement of a micropipette tip pressed against an astrocyte cell body) also initiated Ca^{2+} waves.

The Ca^{2+} waves spread outward radially from the point of stimulation and propagated synchronously in astrocytes and Müller cells. Within the temporal resolution of our measurements (~1 s), Ca^{2+} waves arrived at astrocytes and adjacent Müller cells simultaneously (Fig. 1C). All astrocyte regions, including somata, processes, and end feet, exhibited increased $[Ca^{2+}]_i$ upon arrival of a Ca^{2+} wave, and the propagation of waves was often observed within processes of individual cells. In Müller cells, increases in $[Ca^{2+}]_i$ were observed in cell end feet at the retinal surface and in primary cell processes within the ganglion cell and inner plexiform layers. There was no increase in $[Ca^{2+}]_i$ in cell somata (in the inner nuclear layer), however, indicating that Ca^{2+} waves initiated at the proximal end of Müller cells did not propagate into the distal half of the cell. Movies of glial Ca^{2+} waves can be viewed at http://enlil.med.umn.edu/www/phsl/work/caw.htm.

The time course of the $[Ca^{2+}]_i$ increases observed in astrocytes differed from that in Müller cells (Fig. 1E). In astrocytes, $[Ca^{2+}]_i$ remained elevated for ~10 to 100 s after the arrival of a wave. In Müller cells, in contrast, the arrival of the Ca^{2+} wave often triggered a more transient increase in $[Ca^{2+}]_i$ or initiated a series of $[Ca^{2+}]_i$ oscillations.

The propagation velocities of the Ca^{2+} waves were nearly identical regardless of the stimulus used to initiate them, suggesting that once initiated, the waves were all propagated by the same mechanism. The velocity [measured from wavefront images (Fig. 1D) 1.5 s after stimulation] averaged 25.3 ± 5.4 (mean ± SD, n = 10), 21.9 ± 7.6 (n = 13), and 23.1 ± 6.7 (n = 17) μm/s, respectively, for chemical (ATP), electrical, and mechanical stimuli (Fig. 1F). The propagation velocity slowed as the wave spread outward from the point of stimulation. Calcium increases in both astrocytes and Müller cells were observed at distances as large as 180 μm from the point of stimulation and with latencies as long as 10.6 s.

The increases in $[Ca^{2+}]_i$ observed in astrocytes and Müller cells distant from the site of stimulation might not result from propagated Ca^{2+} waves but perhaps arise from the direct excitation of these cells by the stimulus. The latter explanation is highly unlikely for several reasons. (i) The onset of Ca^{2+} responses in cells distant from the stimulus was usually abrupt and could have latencies as long as 10.6 s. (ii) The propagation velocity of Ca^{2+} waves was nearly identical for chemically, electrically, and mechanically initiated waves. (iii) The Ca^{2+} waves evoked by ejection of ATP did not spread preferentially in the direction of ejection or bath perfusion but rather spread uniformly in all directions.

Additional experiments confirmed that stimuli did not directly trigger Ca^{2+} responses in distant cells. After initiation of a Ca^{2+} wave by mechanical or electrical stimulation, the stimulated astrocyte was refractory

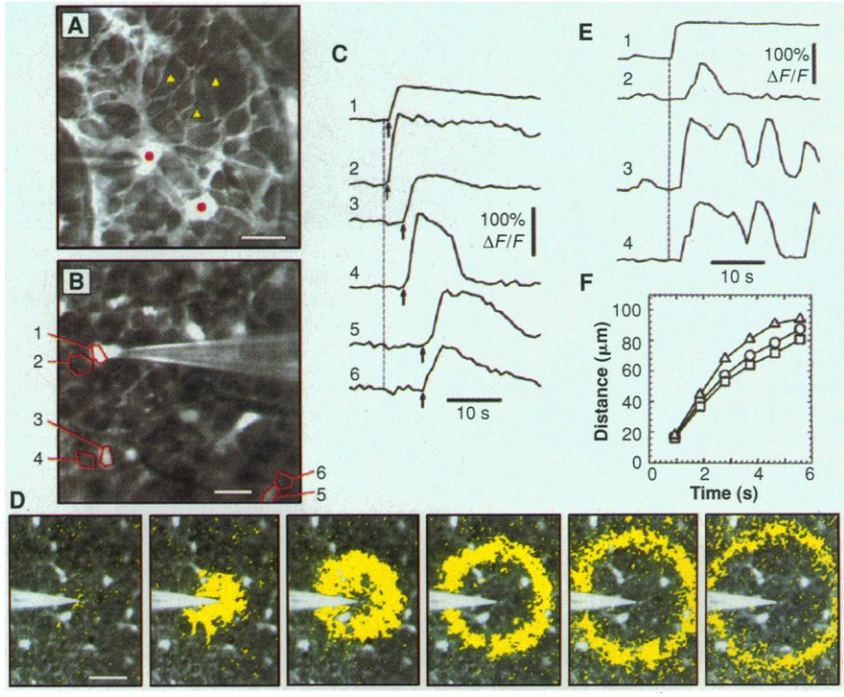

Fig. 1. Propagation of Ca^{2+} waves in glial cells. (**A**) Astrocytes (circles) and end feet of Müller cells (triangles) in a confocal fluorescence image of the vitreal surface of the rat retina labeled with Calcium Green-1. (**B**) The retinal surface with six measurement regions outlined. The stimulating pipette is touching region 1. Regions 1, 3, and 5 outline astrocytes; regions 2, 4, and 6 outline adjacent Müller cell endfeet. (**C**) Change in fluorescence, normalized to baseline fluorescence ($\Delta F/F$), for the six regions in (B). Onset of the mechanical stimulus is indicated by vertical dashed line; arrival of the Ca^{2+} wave is marked by arrows. (**D**) Spread of a Ca^{2+} wave initiated by a mechanical stimulus. The fluorescence image is shown in black and white. Superimposed yellow rings mark the leading edge of the Ca^{2+} wave (where the change in fluorescence between successive panels exceeded a threshold value). Interval between panels, 0.93 s. (**E**) Increases of Ca^{2+} within one astrocyte (trace 1) and three Müller cells (traces 2 through 4), initiated by a mechanical stimulus. (**F**) Propagation velocity of Ca^{2+} waves initiated by mechanical (circles), electrical (squares), and chemical (ATP, triangles) stimuli. Mean distance to the outer edge of the Ca^{2+} wave rings is plotted. Scale bars: (A), 20 μm; (B), 25 μm; and (D), 50 μm.

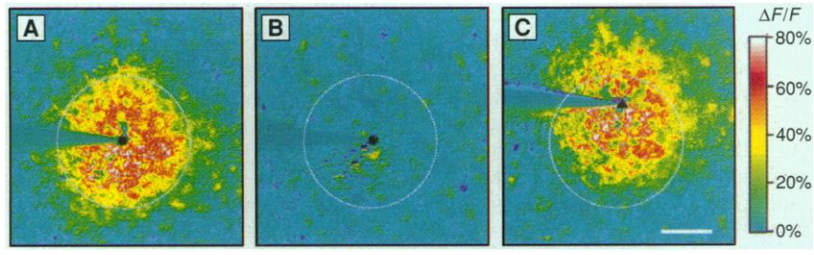

Fig. 2. Normalized fluorescence-difference images of Ca^{2+} waves evoked by repeated stimulation. The pseudocolor images represent a comparison of the mean fluorescence of 15 consecutive images after stimulation and the mean fluorescence of 20 images before stimulation. (**A**) Ca^{2+} wave evoked by a mechanical stimulus. (**B**) Stimulation at the same site (circle) 180 s later elicited no response. (**C**) Ca^{2+} wave evoked by stimulation at a second site (triangle) after an additional 90 s. Dashed circles indicate the response region in (A). Scale bar, 50 μm.

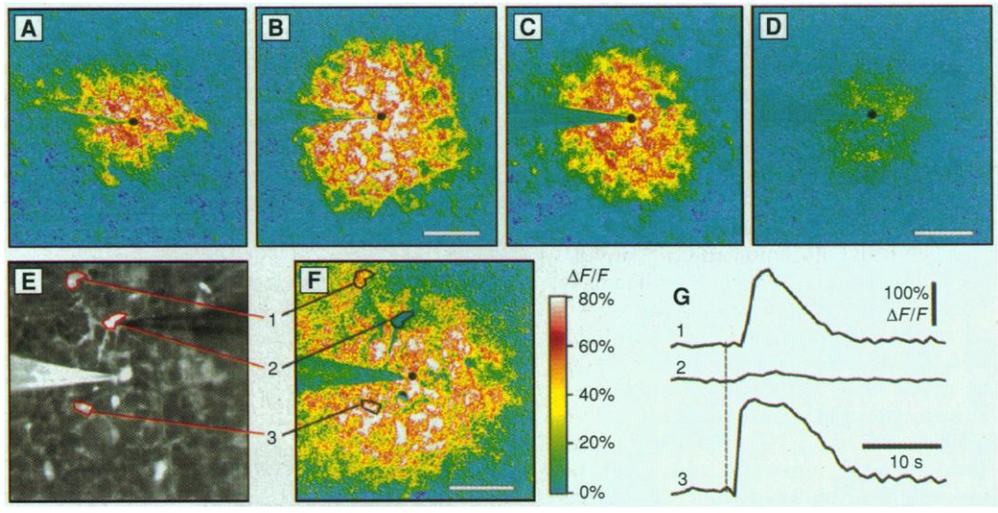

Fig. 3. Generation of Ca^{2+} waves by the release of Ca^{2+} from internal stores. (**A**) Ca^{2+} wave evoked by an electrical stimulus. (**B**) Different region of the retina shown in (A), stimulated after 31 min in 0 mM Ca^{2+} and 0.5 mM EGTA. (**C**) Ca^{2+} wave evoked by an electrical stimulus under control conditions. (**D**) Different region of the retina shown in (C), stimulated 16 min after the addition of 1.5 μM thapsigargin. (**E**) Fluorescence image showing retina, stimulating pipette [left, made visible by coating with DiI (1,1′-dioctadecyl-3,3,3′,3′-tetramethylindocarbocyanine perchlorate)], and patch pipette (right, used to introduce heparin and Calcium Green-1 into the cell). A heparin-containing astrocyte (cell 2) and two untreated astrocytes (cells 1 and 3) are outlined. (**F**) Ca^{2+} wave evoked by ejection of ATP in same retinal area as shown in (E). (**G**) Change in fluorescence of regions shown in (E) and (F). Large $[Ca^{2+}]_i$ increases occurred in untreated cells but not in the heparin-filled cell. Panels (A) through (D) and (F) are normalized fluorescence-difference images. Black circles indicate stimulation sites. Scale bars for all panels, 50 μm.

for several minutes (Fig. 2). During this refractory period, stimulation at the same site initiated a weak, local response or no response at all. However, stimulation of another astrocyte close to the refractory cell initiated a large Ca^{2+} response in the surrounding glial cells (in all 13 trials conducted), demonstrating that these cells were capable of conducting a propagated Ca^{2+} wave.

The propagated increases in $[Ca^{2+}]_i$ in astrocytes and Müller cells apparently arise largely from the release of Ca^{2+} from internal stores, mediated by an inositol 1,4,5-trisphosphate (IP_3) receptor, rather than from an influx of extracellular Ca^{2+}. Normal Ca^{2+} waves were observed when no external Ca^{2+} was present (Fig. 3, A and B). In contrast, bath application of thapsigargin (1.5 μM, for 10 to 16 min), which depletes internal Ca^{2+} stores (*16*), reduced the Ca^{2+} response (Fig. 3, C and D). The Ca^{2+} response was also reduced in cells in which IP_3 receptors were blocked by heparin (*17*) introduced into the cells through a patch pipette (*18*) (Fig. 3, E to G). Astrocytes and Müller cells near heparin-filled cells showed normal Ca^{2+} responses as Ca^{2+} waves swept past. In contrast, the Ca^{2+} response of heparin-treated cells (after 15 min of dialysis) was reduced to 18.7 ± 7.8% (n = 12) of untreated neighboring cells, whereas the Ca^{2+} response of control cells, dialyzed with patch pipette solution without heparin (for an average of 20 min), was 80.3 ± 27.2% (n = 6) of untreated neighbors. The reduction caused by heparin was significantly greater than that caused by dialysis without heparin ($P < 0.0001$, Student's unpaired t test).

The electrophysiological consequences of propagated Ca^{2+} waves were examined. Waves evoked little change in cell membrane potential or input resistance in glial cells, which were monitored in whole cell, current-clamp recordings. Ca^{2+} waves elicited by ejection of ATP were associated with weak depolarizations: 0.15 ± 0.20 mV (n = 19; $P < 0.005$, one-population t test) in astrocytes and 0.16 ± 0.13 mV (n = 20; $P < 0.001$) in Müller cells. Electrical and mechanical stimuli did evoke depolarizations as large as 37 and 8 mV, recorded from astrocytes and Müller cells, respectively. These responses probably represented depolarizations conducted electrotonically from the stimulated cell because (i) the depolarization often occurred before the arrival of the Ca^{2+} wave, (ii) the depolarization was sometimes observed even when the Ca^{2+} wave failed to reach the cell, and (iii) the amplitude of the depolarization declined rapidly as the distance between the stimulation site and the cell increased.

Our results demonstrate that glial cells in freshly excised CNS tissue support the propagation of Ca^{2+} waves. The Ca^{2+} waves we observed resemble those in cultured cells in some respects. The waves have similar propagation velocities (*2*, *5*, *7*, *8*) and both are generated by the release of Ca^{2+} from internal stores (*2*, *4*, *7*), mediated, at least in part, by IP_3 receptors (*19*). In contrast to cultured cells (*2*, *5*), however, astrocytes in the retina were unresponsive to glutamate and did not exhibit oscillations in $[Ca^{2+}]_i$ when stimulated.

Our results further suggest that the propagation of Ca^{2+} waves through astrocytes and Müller cells is linked. Such linkage is consistent with the findings of chemical tracer studies (*20*), which show that astrocytes and Müller cells are coupled. The synchronous spread of Ca^{2+} waves in these cells suggests that, as waves spread outward through the astrocyte syncytium, they may secondarily propagate into Müller cells directly coupled to the astrocytes.

The propagation of calcium waves through a glial syncytium represents an extraneuronal signaling pathway that may influence neuronal activity (*10*, *11*). The absence of membrane potential changes suggests that Ca^{2+} waves do not lead to the voltage activation of ion channels in glial cells, which have been postulated to influence potassium buffering and neurotransmitter uptake (*1*). But an increase in $[Ca^{2+}]_i$ within glial cells could lead to the release of neuroactive substances (*10*, *21*) and to the modulation of neuronal activity.

REFERENCES AND NOTES

1. H. Kettenmann and B. R. Ransom, *Neuroglia* (Oxford Univ. Press, Oxford, 1995).
2. S. M. Finkbeiner, *Glia* **9**, 83 (1993).
3. ———, *Neuron* **8**, 1101 (1992); A. C. Charles *et al.*, *J. Cell Biol.* **118**, 195 (1992).
4. M. O. K. Enkvist and K. D. McCarthy, *J. Neurochem.* **59**, 519 (1992).
5. A. H. Cornell-Bell, S. M. Finkbeiner, M. S. Cooper, S. J. Smith, *Science* **247**, 470 (1990).
6. A. H. Cornell-Bell and S. M. Finkbeiner, *Cell Calcium* **12**, 185 (1991).
7. A. C. Charles, J. E. Merril, E. R. Dirksen, M. J. Sanderson, *Neuron* **6**, 983 (1991).
8. J. W. Dani, A. Chernjavsky, S. J. Smith, *ibid.* **8**, 429 (1992).
9. B. A. Barres, W. J. Koroshetz, L. L. Y. Chun, D. P. Corey, *ibid.* **5**, 527 (1990); J. T. Porter and K. D. McCarthy, *J. Neurochem.* **65**, 1515 (1995); S. Duffy and B. A. MacVicar, *J. Neurosci.* **15**, 5535 (1995); J. T. Porter and K. D. McCarthy, *Glia* **13**, 101 (1995).
10. V. Parpura *et al.*, *Nature* **369**, 744 (1994).
11. M. Nedergaard, *Science* **263**, 1768 (1994); T. D. Hassinger *et al.*, *J. Neurobiol.* **28**, 159 (1995).
12. E. A. Newman and A. Reichenbach, *Trends Neurosci.* **19**, 307 (1996).
13. Retinas from Long-Evans rats were incubated in col-

lagenase/dispase (2 mg/ml) and deoxyribonuclease (DNase) (0.1 mg/ml) for 12 to 20 min before removal of the vitreous humor, then incubated in Calcium Green-1 AM (33.3 mg/ml; Molecular Probes) and pluronic acid (4.7 mg/ml) for 1 hour at room temperature, mounted onto nitrocellulose filters, and secured in a chamber perfused at ~3 ml/min with HCO_3^--buffered Ringer's (24°C) [117 mM NaCl, 3 mM KCl, 2 mM $CaCl_2$, 1 mM $MgSO_4$, 0.5 mM NaH_2PO_4, 15 mM dextrose, 26 mM $NaHCO_3$, equilibrated with 5% CO_2 in O_2 (pH ~7.4)]. In most experiments, 2 μM ATP and 10 or 100 μM glutamate were added to the perfusate to potentiate the Ca^{2+} waves. Ca^{2+} responses were also seen without ATP and glutamate added. Glutamate concentration at the surface of the retina in vivo ranges between 10 and 400 μM [A. A. Heinamaki, A. S. H. Muhonen, R. S. Piha, *Neurochem. Res.* **11**, 535 (1986); G. Gunnarson, A.-K. Jakobbson, A. Hamberger, J. Sjostrand, *Exp. Eye Res.* **44**, 235 (1987)].

14. Labeled glial cells were imaged with a Noran Odyssey confocal scanner and a BX60 Olympus microscope with 20× [0.5 numerical aperture (NA)] and 40× (0.8 NA) water immersion objectives. Calcium Green-1 fluorescence was monitored with 488-nm argon excitation and a 515-nm-long pass barrier filter. Images, averages of 16 video frames, were acquired every 0.93 s with MetaMorph software (Universal Imaging). Measurements were corrected for baseline drift resulting from bleaching.
15. W. T. Kim, M. G. Rioult, A. H. Cornell-Bell, *Glia* **11**, 173 (1994).
16. O. Thastrup, P. J. Cullen, B. K. Drobak, M. R. Hanley, A. P. Dawson, *Proc. Natl. Acad. Sci. U.S.A.* **87**, 2466 (1990).
17. T. K. Ghosh, P. S. Eis, J. M. Mullaney, C. L. Ebert, D. L. Gill, *J. Biol. Chem.* **263**, 11075 (1988).
18. The patch pipette solution contained 5 mM NaCl, 120 mM KCl, 1 mM $CaCl_2$, 7 mM $MgCl_2$, 5 mM EGTA, 5 mM Na_2ATP, 5 mM Hepes, 2 μM Calcium Green-1 K_6 salt, and heparin (100 μg/ml) (6 kD), and the solution was adjusted to pH 7.2 with KOH. Cells were judged to be successfully dialyzed with the pipette solution if Calcium Green-1 fluorescence in the cells increased at least 30% after achieving whole cell recording.
19. Y. Shao and K. D. McCarthy, *Cell Calcium* **17**, 187 (1995); A. C. Charles, E. R. Dirksen, J. E. Merrill, M. J. Sanderson, *Glia* **7**, 134 (1993).
20. S. R. Robinson, E. C. G. M. Hampson, M. N. Munro, D. I. Vaney, *Science* **262**, 1072 (1993).
21. V. Parpura, F. Liu, K. V. Jeftinija, P. G. Haydon, S. D. Jeftinija, *J. Neurosci.* **15**, 5831 (1995).
22. We thank P. Ceelen for technical assistance, M. H. Newman for suggestions concerning data analysis, and J. I. Gepner for helpful comments on the manuscript. Supported by NIH grants EY04077 and EY10383.

12 July 1996; accepted 29 October 1996

Joining the Two Domains of a Group I Ribozyme to Form the Catalytic Core

Michael A. Tanner and Thomas R. Cech*

Self-splicing group I introns, like other large catalytic RNAs, contain structural domains. Although the crystal structure of one of these domains has been determined by x-ray analysis, its connection to the other major domain that contains the guanosine-binding site has not been known. Site-directed mutagenesis and kinetic analysis of RNA splicing were used to identify a base triple in the conserved core of both a cyanobacterial (*Anabaena*) and a eukaryotic (*Tetrahymena*) group I intron. This long-range interaction connects a sequence adjacent to the guanosine-binding site with the domain implicated in coordinating the 5′ splice site helix, and it thereby contributes to formation of the active site. The resulting five-strand junction, in which a short helix forms base triples with three separate strands in the *Tetrahymena* intron, reveals exceptionally dense packing of RNA.

Catalytic RNAs are convenient for investigating how RNA-RNA interactions determine the global folding of the molecule; their structure can be revealed by their activity. In group I introns, RNA forms the active site and directs the cleavage and ligation reactions at the 5′ and 3′ splice sites (*1*). The catalytic core of group I introns consists of two structural domains, P4-P6 and P3-P9 (*2*, *3*). A portion of P4-P6 has been proposed to interact with the substrate helix P1 (*2*, *4*), which contains the 5′ splice site, and P3-P9 contains the binding site for the guanosine nucleophile (*5*). When provided as separate molecules, the P4-P6 and P3-P9 domains of the *Tetrahymena* group I intron can self-assemble into an active structure (*6*). These domains associate with nanomolar apparent dissociation constants, suggesting that they interact through multiple tertiary contacts.

Comparative sequence analysis has been valuable for identifying potential long-range interactions in group I introns (*2*, *7*). Within the transfer RNA (tRNA) subgroup of group I introns, there is a weak triple correlation between the fifth base pair of P4 and the fifth base of J8/7 (*8*) (Fig. 1). All but one have an A·C or G·C base pair at this position in P4, and a G or U nucleotide at J8/7–5. The lone exception, *Azoarcus*, has a C·G base pair and a C at J8/7–5 (*9*, *10*). Although this single example of covariation in the tRNA subgroup is tantalizing, it does not provide substantial evidence for the interaction. Thus, a biochemical approach was undertaken.

The well-characterized tRNA intron from the cyanobacterium *Anabaena* PCC7120 (*11*, *12*) was used to test the importance of base pair 5 in P4 and J8/7 base 5 by site-directed mutagenesis (Fig. 1) (*13*). Orientation of the G·C base pair in P4 was found to be critical because a base pair flip resulted in a rate of splicing that was 2500 times lower (compare Fig. 2, A and B). The J8/7–5 G to U change (found in many tRNA introns) had wild-type activity (*14*), but a G to C change resulted in a 2200 times lower splicing activity (Fig. 2C). When the double mutant of P4 base pair 5 (G·C to C·G) and J8/7–5 (G to C) was tested for splicing, activity was restored; it was only eight times lower than that of wild type, a 300-fold rescue (Fig. 2D). The biphasic kinetics of reaction of the double mutant indicated that it has a residual folding problem (Fig. 3). Restoration of most of the activity with the double mutation sug-

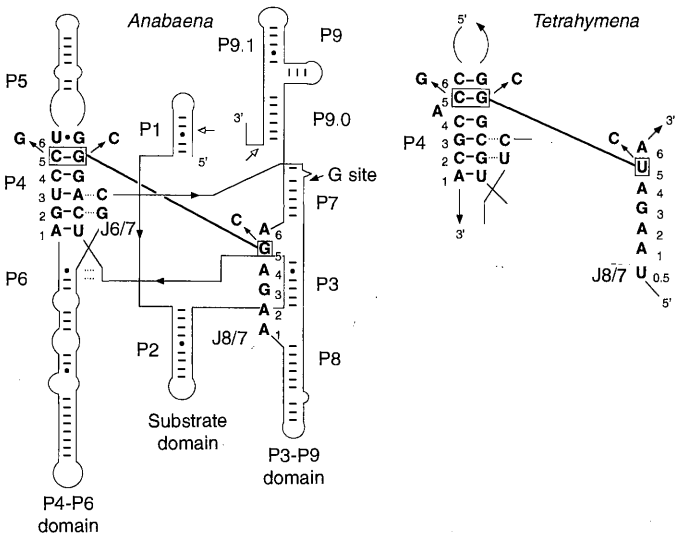

Fig. 1. The secondary structure of the *Anabaena* $tRNA^{Leu}$ intron with the proposed tertiary interaction highlighted. Domain organization (*27*) is shown with splice sites marked by open arrows; the mutations are shown next to the wild-type sequence. P stands for paired region; J stands for joining region; for example, J8/7 joins P8 and P7. (Right) The relevant portions of the *Tetrahymena* ribosomal RNA intron; in this case, P4 contains a bulged A residue not conserved among group I introns.

Department of Chemistry and Biochemistry, Howard Hughes Medical Institute, University of Colorado, Boulder, Colorado 80309-0215, USA.

*To whom correspondence should be addressed.